ACES Asian Chemical Editorial Society

DOI: 10.1002/asia.202100337

CHEMISTRY AN ASIAN JOURNAL Full Paper

Enhanced Peroxidase-mimicking Activity of Plasmonic Gold-modified Mn_3O_4 Nanocomposites through Photoexcited Hot Electron Transfer

Xiaoxuan Han, Rong Liu, Hui Zhang, Quan Zhou, Wei Feng,* and Ke Hu*[a]

Abstract: Enzyme-mimicking artificial nanomaterials often termed nanozymes have broad applications in many fields, including biosensing, pollutant degradation and cancer diagnosis. Herein, we introduce a plasmonic gold nanoparticle-modified Mn_3O_4 nanozyme (Mn_3O_4-Au). Visible or near infrared light excitation into the plasmonic absorption band of the surface-bound gold nanoparticles enhances the catalytic oxidation of tetramethylbenzidine (TMB). The mechanism of light-enhanced peroxidase activity is proposed based on the Mn_3O_4 conduction band mediated hot electron transfer from photoexcited gold nanoparticles to H_2O_2 which undergoes further oxygen-oxygen bond cleavage to yield hydroxyl radical. The surface decoration of plasmonic gold nanoparticles endows Mn_3O_4-Au to be a light-regulated nanozyme.

Introduction

Owing to the characteristics of tuneable catalytic activity and environmental adaptability, nanozymes have been growingly exploited by researchers.[1] Until now, metal oxide-based nanozymes, especially iron,[2] copper,[3] and manganese oxides,[4] have been extensively investigated.[5] Some reports proved that the catalytic activity of nanozymes was closely related to the size,[2b] morphology,[6] surface modification,[5] composition, external energy[4e] and surface microenvironment of nanomaterials.[5] Moreover, the hybrid nanomaterials with unique interfacial interactions were constructed for further enhancing the enzymatic activity.[7] For example, the decoration of Pd NPs on the surface of $CoFe_2O_4$ nanotubes showed the higher catalytic activity of H_2O_2 than the individual Pd NPs and $CoFe_2O_4$ nanotubes.[8] Obviously, the fabrication of metal-oxide-based hybrid nanozymes is an effective means. While the enzymatic activity was promoted, catalytic control becomes the remaining challenge.

To make nanozyme activities tunable, a special "trigger" is needed to adjust the catalytic performance of nanozymes.[9] Using the light, an energy source, nanoparticles absorbed the photon to reach an excited state for achieving challenging photo-chemical reactions.[10] As an external stimulus, photo-irradiation has the properties of non-invasiveness, high temporal and spatial resolution, controllable intensity and wavelength, which can precisely control the catalytic activity. Au nanoparticles (NPs) had unique plasmonic tunability, which effectively adjusted the catalytic activity under the light illumination. Localized surface plasmon resonance generated energetic hot electrons and holes, then the hot electrons with enough energy transferred to react.[11]

Here, we proposed the light-controlled Mn_3O_4-Au nanozymes with plasmonic Au NPs modified on the surface of Mn_3O_4. Upon visible or near IR light excitation into the plasmonic absorption band of Au NPs, hot electrons injected into Mn_3O_4 to promote the generation of hydroxyl radicals (·OH) by single electron reduction of H_2O_2. The participation of ·OH increased the rate of TMB oxidation dramatically. The electron transfer of the light-excited Mn_3O_4-Au nanocomposites improved the peroxidase-mimicking activity.

Results and Discussion

Materials Characterization

Mn_3O_4-Au nanocomposites were prepared by epitaxial growth of manganese oxide on the surface of the gold seed under hydrothermal condition.[11e] The transmission electron microscopic (TEM) image (Figure 1A) of Mn_3O_4-Au nanocomposites showed a uniform composite structure with Mn_3O_4 core about 170 nm diameter and small Au NPs of 20 nm diameter decorated on the surface, which is consistent with the results obtained in DLS (Figure 1B). As shown in Figure 1C, X-ray diffraction (XRD) patterns were performed to differentiate hybrid nanomaterials from Au and Mn_3O_4 alone. The lattice parameters were obtained from the diffraction peaks matched with the PDF card of the Mn_3O_4 (JCPDS# 24-0734) and Au (JCPDS# 04-0784). The diffraction peaks at 38.40° (1 1 1) and 44.50° (2 0 0) correspond to the centered cubic fcc structure and the planes monitored at 28.81° indexed at (1 1 2), 32.63° at (1 0 3) and 50.45° at (1 0 5) were related to the tetragonal crystalline structure of Mn_3O_4. The UV-vis spectroscopy of Mn_3O_4-Au nanocomposites shows the absorption band centred at around 530 nm, which is attributed to the plasmonic absorption of the Au NPs (Figure 1D, Figure S1). Element mapping further confirmed the composition of Mn_3O_4-

[a] X. Han, R. Liu, Dr. H. Zhang, Dr. Q. Zhou, Prof. Dr. W. Feng, Prof. Dr. K. Hu
Department of Chemistry
Fudan University
220 Handan Road, Shanghai
200433 (P. R. China)
E-mail: fengweifd@fudan.edu.cn
khu@fudan.edu.cn

Supporting information for this article is available on the WWW under https://doi.org/10.1002/asia.202100337

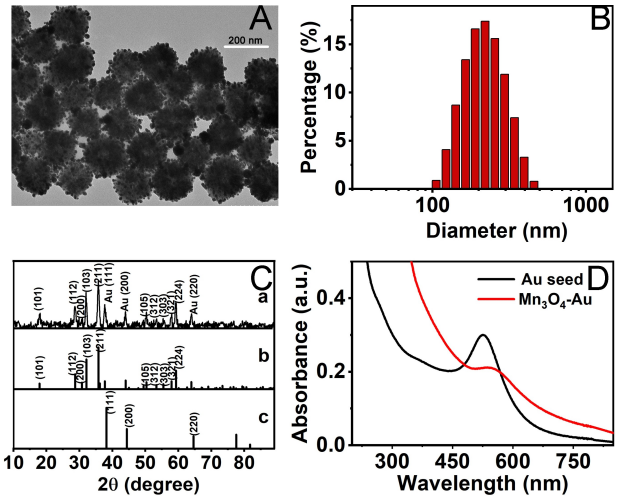

Figure 1. Morphology, size, composition, and optical properties of Mn_3O_4-Au nanozymes. (A) TEM image of Mn_3O_4-Au nanocomposites (scale bar = 200 nm). (B) Hydrodynamic size distribution of Mn_3O_4-Au nanocomposites measured by DLS. (C) X-ray diffraction patterns of the nanoparticles (a. Mn_3O_4-Au nanocomposites, b. PDF card of Mn_3O_4, c. PDF card of Au). (D) UV-vis spectra of Au NPs and Mn_3O_4-Au nanocomposites.

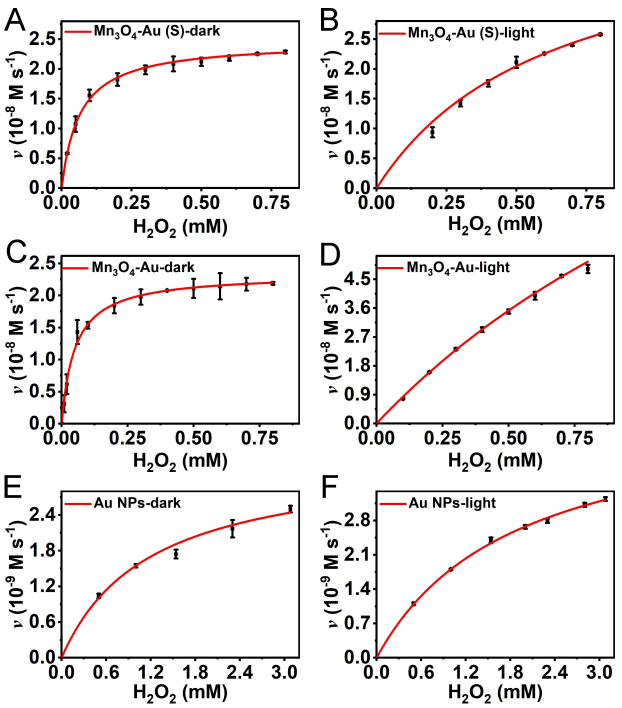

Figure 2. Plots of the initial reaction velocities as a function of the H_2O_2 substrate concentrations for nanozymes of Mn_3O_4-Au (S) nanocomposites (A, B), Mn_3O_4-Au nanocomposites (C, D) and Au NPs (E, F) (pH = 4.5). (The error bars were the standard deviations of 5 independent measurements.) Overlaid in red are non-linear curve fittings based on Michaelis-Menten kinetic model shown in equation 1.

Au nanocomposites with Mn, O, and Au elements (Figure S2). The Mn and O elements were distributed in the central particle, and the Au elements were distributed around the nanoparticles. Hence, the above results indicated that the Mn_3O_4-Au nanocomposites were successfully prepared. The Mn_3O_4-Au (S) nanocomposites were synthesized in a similar way and showed a one-to-one structure (Figure S3).

Kinetic Analysis of Nanozyme Activity

To calculate the peroxidase-mimicking activity of Mn_3O_4-Au (S) nanocomposites, Mn_3O_4-Au nanocomposites and Au NPs, the colorimetric method based on TMB oxidation was used. By this way, H_2O_2 oxidizes colourless TMB under the catalysis with a characteristic absorption peak of TMB_{ox} at 652 nm. In acidic conditions (pH = 4.5), nanozyme as the catalyst split H_2O_2 into ·OH and H_2O. Without the TMB, the ·OH adsorbed on the surface of the nanozyme tightly and initiated the reverse reaction until the reaction equilibrium state was formed. Based on the hypothesis, the kinetic parameters were obtained. The reaction kinetic parameter was calculated according to the Michaelis-Menten Equation:

$$v = \frac{v_{max} \times [S]}{K_M + [S]} \quad (1)$$

Where v is the initial reaction velocity, v_{max} is maximal reaction velocity, K_M is the Michaelis constant and $[S]$ is the substrate concentration. In addition, v_{max} and K_M can also be obtained by the Hanes-Woolf plot:

$$\frac{[S]}{v} = \frac{[S]}{v_{max}} + \frac{K_M}{v_{max}} \quad (2)$$

in which the slope of a straight diagonal line is $1/v_{max}$, and the intercept of the vertical axis is K_M/v_{max}. The catalytic constant $k_{cat} = v_{max}/[E]$, where [E] is the catalyst concentration. Catalytic efficiency $\eta = k_{cat}/K_M$.

As shown in Figure 2, with the increase of the concentration of H_2O_2, the initial reaction rate (v_0) was increased obviously at the preliminary stage. Nevertheless, owing to the saturation of the active sites on the surface of Mn_3O_4-Au nanocomposites, the v_0 reached the maximum when the dose of substrate was high enough, which is similar to the catalytic process of natural enzymes. Derived from this phenomenon, the Michaelis-Menten equation was used to fit of the v_0 and H_2O_2 concentration. The kinetic parameters (K_M, v_{max}, k_{cat}, k_{cat}/K_M) were obtained based on the formula 1 and showed in Table 1. In the dark, the K_M of Au NPs was about 10 times higher than that of Mn_3O_4-Au nanocomposites, while the K_M of Mn_3O_4-Au (S) nanocomposites and Mn_3O_4-Au nanocomposites had no obvious changes. It was induced by the higher affinity of Mn_3O_4 to H_2O_2. After the irradiation of 532 nm laser, collisional electron transfer led to the enhancement of the K_M. Besides, in the dark, all parameters of the Mn_3O_4-Au (S) nanocomposites and Mn_3O_4-Au nanocomposites were roughly the same. In contrast to the catalysis of nanozyme which always showed a static binging of substrates, the photocatalysis process need more substrate to avoid the recombination of electrons and holes, which was consistent with the change of the specificity constant η (k_{cat}/K_M). The decrease of the k_{cat}/K_M indicates the increase of diffusion effect. An obvious

Table 1. Fitting and derived parameters from Hanes-Woolf plots of the Mn_3O_4-Au (S) nanocomposites, Mn_3O_4-Au nanocomposites and Au NPs with H_2O_2 as the substrate.

H_2O_2	Mn_3O_4-Au (S)		Mn_3O_4-Au		Au NPs	
	dark	light	dark	light	dark	light
K_M (mM)	0.065	0.63	0.050	2.1	1.2	1.9
v_{max} (10^{-8} M s^{-1})	2.5	4.6	2.3	18	0.34	0.52
k_{cat} (10^3 s^{-1})	5.9	11	5.6	43	0.80	1.2
η (10^7 M^{-1} s^{-1})	9.1	1.8	11	2.1	0.068	0.066

Table 2. Fitting and derived parameters from Hanes-Woolf plots of the Mn_3O_4-Au (S) nanocomposites, Mn_3O_4-Au nanocomposites and Au NPs with TMB as the substrate.

TMB	Mn_3O_4-Au (S)		Mn_3O_4-Au		Au NPs	
	dark	light	dark	light	dark	light
K_M (mM)	0.49	0.16	0.41	0.51	0.61	0.81
v_{max} (10^{-8} M s^{-1})	1.8	1.4	1.7	5.7	0.050	0.042
k_{cat} (10^3 s^{-1})	4.0	3.3	4.0	14	0.12	0.13
η (10^7 M^{-1} s^{-1})	0.88	2.1	0.95	2.7	0.20	0.16

increase of k_{cat} under illumination could be found, which is resulting from the light-induced electron transfer from nanomaterials to H_2O_2. Under the 532 nm laser irradiation, the catalyst activity of the Mn_3O_4-Au nanocomposites enhanced significantly, which was proved by the k_{cat} of Mn_3O_4-Au nanocomposites with three times higher photon absorption than that of Mn_3O_4-Au (S) nanocomposites.

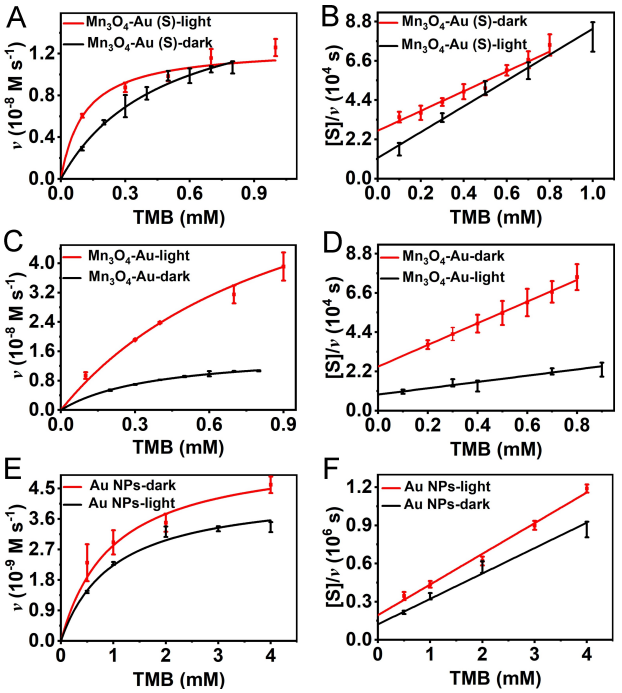

Figure 3. Plots of the initial reaction velocities as a function of the TMB substrate concentrations for nanozymes of Mn_3O_4-Au (S) nanocomposites (A), Mn_3O_4-Au nanocomposites (C) and Au NPs (E) under dark and light conditions. Overlaid in red and black under dark and light conditions (A, C, E) are non-linear curve fittings based on Michaelis-Menten kinetic model shown in equation 1. Data linearization of the Michaelis-Menten equation to Hanes-Woolf plots of Mn_3O_4-Au (S) nanocomposites (B), Mn_3O_4-Au nanocomposites (D) and Au NPs (F) based on equation 2 are also shown.

TMB as another substrate was used to quickly scavenge ·OH and induce the separation of intermediate product. As shown in Figure 3 and Table 2, the kinetic parameters were also not significantly different between the Mn_3O_4-Au (S) nanocomposites and Mn_3O_4-Au nanocomposites in the dark. Under 532 nm laser irradiation, the v_{max} and k_{cat} of Mn_3O_4-Au nanocomposites increased by 3-fold, while those of Mn_3O_4-Au (S) nanocomposites were within experimental error the same. The above phenomenon is consistent with that of H_2O_2. The collective kinetic results exhibit that compared with Mn_3O_4-Au (S) nanocomposites, the peroxidase-mimicking catalytic activity of Mn_3O_4-Au nanocomposites that comprise more Au NPs per Mn_3O_4 NP is significantly improved under light conditions. Besides, both the Mn_3O_4-Au nanocomposites and horseradish peroxidase (HRP) were tested at 25–60 °C or pH 2–11 and measured under the same conditions. Compared with the HRP, Mn_3O_4-Au nanocomposites has better stability over wide ranges of pH and temperature (Figure S4).

Photocatalysis Reaction Process of Mn_3O_4-Au Nanocomposites

On the basis of the kinetic results, a possible catalytic mechanism was proposed. Under the visible light irradiation, the hot electron-hole pairs were produced by Au NPs. These photogenerated hot electrons are known to have very short lifetimes on the scale of picoseconds. Fortunately, as the Au NPs were attached on the surface of Mn_3O_4 nanoparticles, the hot electrons from Au NPs injected into the conduction band of Mn_3O_4 which suppressed rapid hot electron relaxation and recombination within Au NPs. The conduction band minimum of Mn_3O_4 was previously determined to be −0.9 V[12a] while the redox potential of the one electron reduction of H_2O_2 was 0.8 V vs. NHE.[12b] The driving force for photoreduction of H_2O_2 is as large as 1.7 V. We propose that the injected electrons were mediated by the conduction band of Mn_3O_4 and further transferred to H_2O_2 to induce the O–O bond dissociation of H_2O_2 to ·OH and OH^- as

shown in Scheme 1. Finally, holes of the Au NPs were filled by OH^- anions, water molecules or other electron donors in the aqueous environment.[13]

The apparent quantum yield (AQE) of the photo-enhanced peroxidase-mimicking catalytic reaction was calculated according to the formula 2 and showed in Figure 4A. Compared with the Au NPs alone, AQE in Mn_3O_4-Au nanocomposites was significantly improved, which may be attributed to the efficient electron transfer from Au NPs to Mn_3O_4. In order to further confirm if the enhanced peroxidase mimicking photocatalysis was originated from plasmonic excitation of surface decorated gold nanoparticles, the Mn_3O_4-Au (S) nanocomposites were excited by different wavelengths with the same number of photons. When switching λ_{ex} from 532 nm to 405, 450, 655 and 808 nm, the reaction became significantly slower (Figure 4B).

Indeed, the AQE at different wavelengths of excitation carefully followed the plasmonic absorption spectrum of Au NPs (Figure 4C). DMPO was chosen as a spin trap to form the spin adduct which can confirm the existence of hydroxyl free radicals (·OH). Electron spin resonance (ESR) spectra has four lines with relative intensities of 1:2:2:1. It further confirmed that ·OH was produced in the reaction. After 532 nm laser irradiation, the increase of ESR signal indicated a higher production of ·OH during the reaction and proved that the light promoted the production of reactive oxygen species (ROS) (Figure 4D).

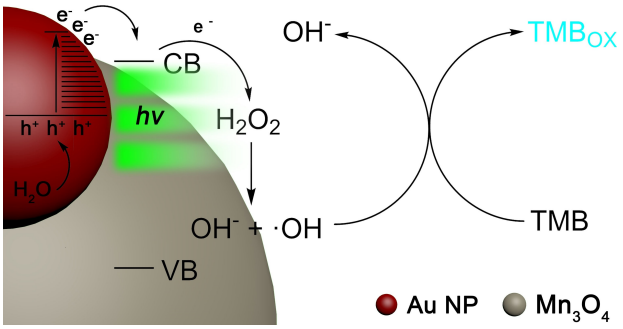

Scheme 1. Illustration of the working mechanism of peroxidase-mimicking Mn_3O_4-Au nanozyme.

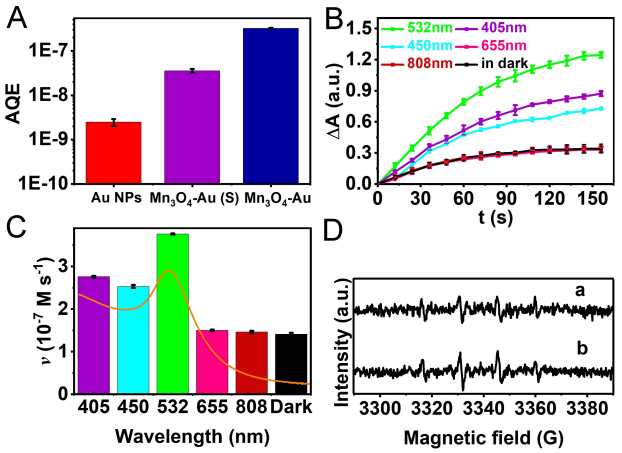

Figure 4. (A) AQE of Au NPs, Mn_3O_4-Au (S) nanozyme, Mn_3O_4-Au nanozyme. (B) Absorption change of 532 nm, 405 nm, 450 nm, 655 nm, 808 nm as the function of time of Mn_3O_4-Au catalysed TMB oxidation to the different wavelength of light. (C) ν_0 in dark and under laser illumination at λ_{ex} of 405, 450, 532, 655 and 808 nm. The initial concentrations of Mn_3O_4-Au nanozymes, H_2O_2, and TMB were fixed at 500 μM, 10 mM, 10 mM, respectively. (orange curve: plasmonic absorption spectrum of Au NPs.) (D) ESR spectra of ·OH spin adduct generated by Mn_3O_4-Au nanozyme (a. in the dark, b. under 532 nm laser irradiation).

Conclusion

To summarize, we synthesized plasmonic Au NP-coated Mn_3O_4-Au nanozymes with superior photo-enhanced peroxidase-mimicking activities. Based on this phenomenon as well as fitting of the Michaelis-Menten kinetic model, the reaction mechanism of this nanozyme was proposed. The hot electrons generated by visible light are transferred from Au NPs to Mn_3O_4, which promotes the decomposition of H_2O_2 into hydroxide ions and hydroxyl radicals. In this way, peroxidase substrate like TMB can be oxidized at a rate dictated by light as an external control. The binary nanocomposite materials based on plasmonic Au sensitization to a known nanozyme like Mn_3O_4 open a door to even higher reactivities of nanostructured enzyme mimics.

Experimental Section

Materials

Manganese (II) acetate tetrahydrate ($Mn(CH_3COO)_2{\cdot}4H_2O$, 98%), Gold (III) chloride trihydrate ($HAuCl_4{\cdot}3H_2O$, 99%, Au:50%), 3,3′,5,5′-tetramethyl benzidine (TMB, 10 mM, 98%) and H_2O_2 (30%) were obtained from Adamas. Poly(vinyl pyrrolidone) (PVP, Mw = 40,000 $g{\cdot}mol^{-1}$) and horseradish peroxidase (HRP) were purchased from Sigma-Aldrich. Hydrazine hydrate aqueous solution was acquired from Chinese Medicines Group Chemical Reagent Co. Ltd. Acetate buffer was purchased from Coolaber. All the chemicals were analytical grade and used without further purification. All aqueous solutions were prepared with doubly distilled water.

Instrumentations

UV-vis spectra were measured by a UV-vis spectrophotometer (Agilent Cary 60). The X-ray diffraction (XRD) pattern for Mn_3O_4-Au nanocomposites was obtained on a Bruker D2 PHASER X-ray diffractometer using Cu Kα (λ = 1.5418 Å) as the source. Dynamic light-scattering (DLS) measurements were performed on a Nano ZS Malvern Zeta sizer instrument (Zetananosizer ZS-90). The morphological microstructure was characterized by JEM-1400, JEOL transmission electron microscopy (TEM) model, operated at 120 kV. HR scaning electron microscopy (SEM) measurements were conducted on Tecnai G2 F20 S-Twin HR-SEM (FEI, Hillsboro, OR, USA). The ESR spectrum was implemented by a BrukerEMX plus model spectrometer operating at X-band frequencies (9.8 GHz) at ambient temperature. pH values were measured by a pH meter (Mettler Toledo, FiveEasy Plus). All the experiments were performed at room temperature.

Preparation of Mn_3O_4-Au Nanocomposites

Briefly, Mn_3O_4-Au nanocomposites were synthesized as described previously.[11e] PVP (20 mM) and $HAuCl_4{\cdot}3H_2O$ (0.5 mM) were added

to a 100 mL aqueous solution, refluxing (ca. 100 °C) for 10 min, and then an aqueous solution of $N_2H_4{\cdot}H_2O$ was added quickly. The reaction was continued for another 30 min. At this time, Au nanoparticles were obtained. PVP and Mn $(Ac)_2{\cdot}4H_2O$ were added to a 90 mL aqueous ethanolic solution, refluxing (ca. 80 °C) for 10 min, and then 10 mL solution of Au nanoparticles was added dropwise over the course of 10 min. The reaction proceeded for another 2 h. By adjusting the solvent ratio in the reaction, we obtained two nanocomposites designated as Mn_3O_4-Au and Mn_3O_4-Au (S), where S in the parentheses meant that less than a single gold nanoparticle was on each Mn_3O_4 nanoparticle. The solvent ratios of the aqueous ethanolic solution were H_2O: ethanol = 3:1 and 1:1, respectively.

Michaelis-Menten Kinetic Analysis

To examine the influence of light irradiation, Mn_3O_4-Au nanocomposites (0.05 mg/mL, 100 μL), H_2O_2 and TMB were added into 800 μL of 0.1 M acetate buffer with the light irradiation of 532 nm (366 mW/cm^2). The total volume of reaction system was kept at 1.2 mL. When using TMB or H_2O_2 as the substrate, the substrate concentration all selected as 10 mM. The reaction was incubated at 37 °C. When the HRP was detected, Mn_3O_4-Au nanocomposites were replaced by HRP, and the others remained unchanged. The initial enzymic reaction velocity of TMB was obtained by monitoring the absorbance at 652 nm for 2 min. The concentration of oxidized TMB (TMB_{ox}) was calculated from Beer-Lambert Law. All kinetic measurements were repeated 5 times and the error bars were the standard deviations of 5 independent measurements.

The laser sources of 405 nm, 450 nm,532 nm,655 nm and 808 nm output the same number of photos in the reaction. The number of photos was calculated according to the following equation 3.

$$\lambda P = \frac{hcN}{t} \tag{3}$$

where P is the power, λ is the wavelength, h is the Planck constant, N is the number of photos, c is the speed of the light and t is the time. Under illumination at the same time, the product of wavelength and power was keeping the same, and the same number of photons can be obtained.

We calculated the apparent quantum efficiency (AQE) using the following equation:

$$\mathrm{AQE} = \frac{\{\ h \times c \times V \times N_A \times\ [v_0(\text{laser on}) - v_0(\text{laser off})]\}}{P_{ex} \times \lambda_{ex}} \tag{4}$$

Where h is the Plank constant, c is the speed of light in air, V is the volume of the reaction system, and N_A is the Avogadro's number. v_0 (laser on) is the initial reaction velocities under laser illumination and v_0 (laser off) is the initial reaction velocities in dark.

Acknowledgements

The authors thank the National Natural Science Foundation of China (Grant 21872037) for financial support.

Conflict of Interest

The authors declare no conflict of interest.

Keywords: gold modified Mn_3O_4 · photo-enhanced · peroxidase-mimicking · plasmonic · electron transfer

[1] a) J. Lv, C. Zhang, S. Wang, M. Li, W. Guo, *Analyst* **2021**, *146*, 605–611; b) W. Song, B. Zhao, C. Wang, Y. Ozaki, X. Lu, *J. Mater. Chem. B* **2019**, *7*, 850–875; c) K. Herget, P. Hubach, S. Pusch, P. Deglmann, H. Gotz, T. E. Gorelik, I. A. Gural'skiy, F. Pfitzner, T. Link, S. Schenk, M. Panthofer, V. Ksenofontov, U. Kolb, T. Opatz, R. Andre, W. Tremel, *Adv. Mater.* **2017**, *29*; d) A. Asati, S. Santra, C. Kaittanis, S. Nath, J. M. Perez, *Angew. Chem. Int. Ed.* **2009**, *48*, 2308–2312; *Angew. Chem.* **2009**, *121*, 2344–2348.

[2] a) H. Wei, E. Wang, *Anal. Chem.* **2008**, *80*, 2250–2254; b) L. Gao, J. Zhuang, L. Nie, J. Zhang, Y. Zhang, N. Gu, T. Wang, J. Feng, D. Yang, S. Perrett, X. Yan, *Nat. Nanotechnol.* **2007**, *2*, 577–583.

[3] a) A. L. Hu, Y. H. Liu, H. H. Deng, G. L. Hong, A. L. Liu, X. H. Lin, X. H. Xia, W. Chen, *Biosens. Bioelectron.* **2014**, *61*, 374–378; b) L. Hong, A. L. Liu, G. W. Li, W. Chen, X. H. Lin, *Biosens. Bioelectron.* **2013**, *43*, 1–5; c) W. Chen, J. Chen, A. L. Liu, L. M. Wang, G. W. Li, X. H. Lin, *ChemCatChem* **2011**, *3*, 1151–1154.

[4] a) B. Ding, P. Zheng, P. Ma, J. Lin, *Adv. Mater.* **2020**, *32*, e1905823; b) Z. W. Kang, R. K. Kankala, B. Q. Chen, C. P. Fu, S. B. Wang, A. Z. Chen, *ACS Appl. Mater. Interfaces* **2019**, *11*, 28781–28790; c) J. Zhang, X. Lu, D. Tang, S. Wu, X. Hou, J. Liu, P. Wu, *ACS Appl. Mater. Interfaces* **2018**, *10*, 40808–40814; d) J. Yao, Y. Cheng, M. Zhou, S. Zhao, S. Lin, X. Wang, J. Wu, S. Li, H. Wei, *Chem. Sci.* **2018**, *9*, 2927–2933; e) C. Wang, Q. Zhang, X. Wang, H. Chang, S. Zhang, Y. Tang, J. Xu, R. Qi, Y. Cheng, *Angew. Chem. Int. Ed.* **2017**, *56*, 6767–6772; *Angew. Chem.* **2017**, *129*, 6871–6876; f) W. Li, Z. Liu, C. Liu, Y. Guan, J. Ren, X. Qu, *Angew. Chem. Int. Ed.* **2017**, *56*, 13661–13665; *Angew. Chem.* **2017**, *129*, 13849–13853.

[5] H. Wei, E. Wang, *Chem. Soc. Rev.* **2013**, *42*, 6060–6093.

[6] a) C. Ge, R. Wu, Y. Chong, G. Fang, X. Jiang, Y. Pan, C. Chen, J.-J. Yin, *Adv. Funct. Mater.* **2018**, *28*; b) C. Ge, G. Fang, X. Shen, Y. Chong, W. G. Wamer, X. Gao, Z. Chai, C. Chen, J. J. Yin, *ACS Nano* **2016**, *10*, 10436–10445.

[7] S. Sahar, A. Zeb, C. Ling, A. Raja, G. Wang, N. Ullah, X. M. Lin, A. W. Xu, *ACS Nano* **2020**, *14*, 3017–3031.

[8] Z. Yang, Z. Zhang, Y. Jiang, M. Chi, G. Nie, X. Lu, C. Wang, *RSC Adv.* **2016**, *6*, 33636–33642.

[9] a) Y. Liu, X. Wang, H. Wei, *Analyst* **2020**, *145*, 4388–4397; b) S. Wu, J. Zhang, P. Wu, *Anal. Methods* **2019**, *11*, 5081–5088; c) B. Liu, J. Liu, *Nano Res.* **2017**, *10*, 1125–1148.

[10] a) J. Zhang, S. Wu, X. Lu, P. Wu, J. Liu, *Nano Lett.* **2019**, *19*, 3214–3220; b) Y. Huang, J. Ren, X. Qu, *Chem. Rev.* **2019**, *119*, 4357–4412; c) Y. Guo, X. Li, Y. Dong, G.-L. Wang, *ACS Sustainable Chem. Eng.* **2019**, *7*, 7572–7579; d) M. Y. Ho, G. Shen, D. P. Canniffe, C. Zhao, D. A. Bryant, *Science* **2016**, *353*; e) C. M. Courtney, S. M. Goodman, J. A. McDaniel, N. E. Madinger, A. Chatterjee, P. Nagpal, *Nat. Mater.* **2016**, *15*, 529–534; f) X. Lang, X. Chen, J. Zhao, *Chem. Soc. Rev.* **2014**, *43*, 473–486; g) C. Chen, W. Ma, J. Zhao, *Chem. Soc. Rev.* **2010**, *39*, 4206–4219; h) J. Zhang, J. Liu, *Nanoscale* **2020**, *12*, 2914–2923.

[11] a) Y. Zhang, E. Villarreal, G. G. Li, W. Wang, H. Wang, *J. Phys. Chem. Lett.* **2020**, *11*, 9321–9328; b) M. L. Brongersma, N. J. Halas, P. Nordlander, *Nat. Nanotechnol.* **2015**, *10*, 25–34; c) A. O. Govorov, H. Zhang, H. V. Demir, Y. K. Gun'ko, *Nano Today* **2014**, *9*, 85–101; d) M. J. Kale, T. Avanesian, P. Christopher, *ACS Catal.* **2013**, *4*, 116–128; e) S. K. Ghosh, J. Kang, M. Inokuchi, N. Toshima, *Appl. Catal. A* **2013**, *464–465*, 225–232.

[12] a) N. Li, Y. Tian, J. H. Zhao, J. Zhang, J. Zhang, W. Zuo, Y. Ding, *Appl. Catal. B* **2017**, *214*, 126–136; b) J. J. Warren, T. A. Tronic, J. M. Mayer, *Chem. Rev.* **2010**, *110*, 6961–7001.

[13] C. Wang, Y. Shi, Y. Y. Dan, X. G. Nie, J. Li, X. H. Xia, *Chem. Eur. J.* **2017**, *23*, 6717–6723.

Manuscript received: March 31, 2021
Revised manuscript received: April 27, 2021
Accepted manuscript online: April 28, 2021
Version of record online: May 11, 2021